

Numerical modeling of the CO₂ desorption process coupled with phase transformation and heat transfer in a CCS installation

Paweł Niegodajew*, Dariusz Asendrych, Stanisław Drobniak

Institute of Thermal Machinery

Częstochowa University of Technology, Poland

Abstract

The paper concerns research aimed at developing a computational fluid dynamics (CFD) model of an amine-based carbon dioxide capture process in post-combustion capture (PCC) technology. A numerical model of the absorber column (the first stage of PCC cycle) including complex hydrodynamics, heat transfer and absorption reaction involving monoethanolamine (MEA) was developed and described in detail in [1, 2]. This paper focuses on the second stage of the PCC cycle: the desorber (stripper) column. An Eulerian multiphase model was adopted to resolve two-phase counter-current gas-liquid flow in a porous region with desorption reaction, multiphase heat transfer and evaporation/condensation phenomena. The preliminary calculations were performed on simplified geometry of the stripper column in order to reduce the computational time required. The results showed physically correct behavior, proving its relevance and utility for practical applications.

Keywords: post combustion, CCS, desorption, stripper, MEA, CFD introduction

1. Introduction

The post-combustion capture approach is considered to be one of the most mature techniques for CO₂ separation of the carbon capture and storage (CCS) technologies available. This method has been tested in pilot plant scale installations [3–8] all over the world and has already been scaled up to demonstration plant level [9].

In PCC technology CO₂ is recovered from flue gases by an aqueous solvent solution. The most commonly-used solvent in this separation technology is MEA, mostly due to its high reactivity performance [7], there are also other alternatives during developing [10, 11].

The general process diagram is presented in Fig. 1. The aqueous amine solvent solution is delivered at the top of the absorber column, whereas the flue gases enter the column at the bottom. Both phases flow counter-currently through the packing section, ensuring an enlarged contact area between the phases and faster reaction in this region. CO₂-free flue gases leave the absorber column at the top while loaded amine leaves the column at the bottom and flows through the heat exchanger into the stripper section. In this section (the object of this article) the loaded amine flows downstream in the desorber column through the porous zone and is collected in the tank located at the bottom of the column, where due to the additional heat supplied, the absorption reaction is reversed and CO₂ is released. The amine in the tank is heated up to a temperature exceeding 100°C. Such a high temperature causes evaporation

*Corresponding author

Email address: niegodajew@gmail.com (Paweł Niegodajew*)

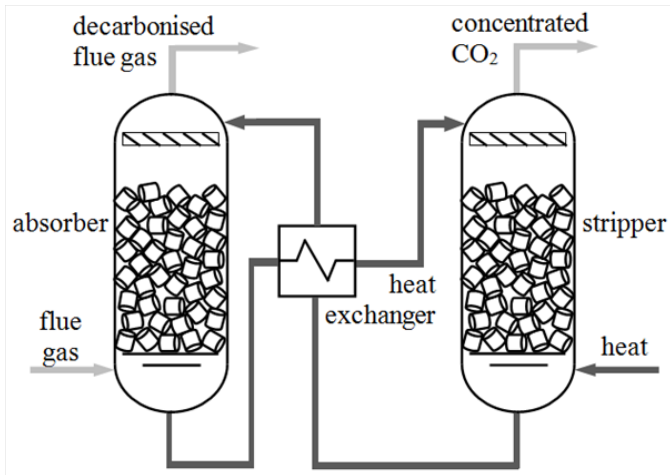


Figure 1: The process flow diagram for CO₂ capture in a post-combustion method

of the water solution with amine solvent. Consequently, the water vapor together with released carbon dioxide starts to flow counter-currently with rich amine solvent in the porous zone and exchange heat. Most of the water vapor condenses along the column, whereas the rest will leave the column together with CO₂ at the stripper top. Therefore, an additional condenser section is required to turn the vapor back to the desorber. Amine without CO₂ leaves the stripper column at the bottom and flows through the heat exchanger to the absorber, where the cycle starts to repeat.

The PCC technology described above involves several complex phenomena (two-phase flow, endo-/exothermic chemical reactions, evaporation/condensation, interphase heat transfer, liquid holdup in the porous zone, etc.) coupled together and affecting the CO₂ capture process. Experimental analysis performed on pilot plant installations are unable to investigate the influence of single phenomenon on CO₂ capture process.

Numerical analysis can provide a detailed description of the entire process and that hence experimental investigations are frequently supported by numerical simulation. There are numerous research groups working on numerical modeling of PCC processes by means of simplified 0D or 1D models [12–16], but these simplified models are unable to provide a detailed description of the process and hence identify weak points requiring improvement.

The Computational Fluid Dynamics (CFD) model

proposed in this paper, is able to provide an insight into the details of the process. In particular, this approach allows one to perform extensive parametric studies in order to formulate optimization guidelines, which are of major importance from the viewpoint of PCC cost reduction.

Due to its high complexity, the CFD model of the PCC process was developed in steps. At first the numerical model of counter-current two-phase gas-liquid flow was proposed [1] and then extended by CO₂ absorption process chemistry and thermodynamics [2]. In the present paper the second PCC step is considered, covering simulation of CO₂ release in a stripper column.

2. Numerical model

The CFD model was developed using commercial software ANSYS FLUENT. All modifications performed in code (e.g., mass, momentum or energy source terms) were made using the researchers' own subroutines written in C++ programming language.

2.1. Governing equations

The physical phenomena occurring in the stripper column can be described by the system of Navier-Stokes equations. In the multiphase two-fluid Euler-Euler model this system of equations is solved separately for each phase. Mass conservation for k^{th} phase takes the form

$$\frac{\partial}{\partial t} (\alpha_k \rho_k) + \nabla (\alpha_k \rho_k \bar{u}_k) = S_k \quad (1)$$

where \bar{u}_k is flow velocity, ρ_k phase density and S_k is a mass source term corresponding to species production/destruction due to chemical reaction and/or phase change. A momentum equation with respect to the Eulerian multiphase model (assuming flow incompressibility) takes the following form:

$$\frac{\partial}{\partial t} (\alpha_k \rho_k \bar{u}_k) + \nabla (\alpha_k \rho_k \bar{u}_k \bar{u}_k) = -\alpha_k \nabla p + \nabla^2 (\alpha_k \mu_k \bar{u}_k) + \alpha_k \rho_k \bar{g}_k + \bar{F}_k \quad (2)$$

In the above equation p is the static pressure shared by all phases, μ_k is the dynamic viscosity and g_k is gravitational acceleration. Phase interaction force F_k is defined using the Schiller-Naumann

formula [17], a Fluent default mechanism, which is however appropriate for the dispersed liquid phase only. Therefore it was applied for the stripper sections outside the porous zone. In a packing bed section, liquid flows as a thin film covering filling elements and the phase interaction mechanism changes qualitatively. Thus force F_k equals zero in this region and its function is taken over by a source term $S_{pz,k}$. It is dependent on phase fluxes and fluids' properties, and also on the type and size of packing elements. The relevant formulas allowing to determine the term $S_{pz,k}$ as well as liquid holdup were adopted from the work of Maćkowiak [18] which is a comprehensive study of packed beds.

As the stripper column is a chemically reacting system, additional equations have to be included in the model. The general transport equation of i^{th} species in multiphase flow is given as

$$\frac{\partial}{\partial t} (\alpha_k \rho_k Y_{i,k}) + \nabla (\alpha_k \rho_k \bar{u}_k Y_{i,k}) = -\nabla \alpha_k \bar{J}_{i,k} + R_i \quad (3)$$

where $Y_{i,k}$ is mass fraction, R_i stands for heterogeneous reaction rate. $\bar{J}_{i,k}$ is a stream of i^{th} species diffused, and for laminar flow conditions it can be modeled by Fick's law.

The CO₂ capture process involves intense energy transfer resulting from chemical reaction, phase change phenomena and rich MEA heating in the stripper. Energy transfer in the Eulerian model is described separately for each phase by the enthalpy transport equation:

$$\frac{\partial}{\partial t} (\alpha_k \rho_k h_k) + \nabla (\alpha_k \rho_k \bar{u}_k h_k) = \alpha_k \frac{\partial p}{\partial t} + \nabla (\lambda_k \nabla T_k) + Q_k + S_{e,k} \quad (4)$$

where h_k is specific enthalpy, λ_k is thermal conductivity, Q_k is the intensity of heat exchange between phases and $S_{e,k}$ is the enthalpy source term due to chemical reaction and/or phase change phenomena. Further details of the model may be found in [1, 2].

2.2. Desorption chemistry

The chemistry of the CO₂ absorption/desorption by aqueous monoethanolamine solution is regarded as a reversible reaction [19] of the form:



resulting in the formation of an MEA-carbamate (first term on the r.h.s.) and a protonated MEA (second term on the r.h.s.) named jointly as loaded MEA or rich MEA. In above reaction R represents an alcohol group (CH₂)₂OH⁻. The expression 5 neglects the presence of ions (like H₃O⁺, OH⁻, CO₃²⁻) as their content for CCS installations working on fossil fuels with MEA as a solvent is negligible [12, 19]. The mass rate of i^{th} chemical species produced due to the second-order reaction is given by:

$$R_i = M_i \cdot k_b \cdot C_{MEA-H} \cdot C_{MEA-CO_2} \quad (6)$$

where M_i is molecular weight, k_b is backward reaction rate constants and C_{MEA-H} / C_{MEA-CO_2} are molar concentrations of reacting media. The reaction rate constants can be described by the following temperature-dependent expression:

$$k_b = 4.3 \cdot 10^{11} \exp(-80.8/(RT)) \quad (7)$$

adopted from [20].

2.3. Boundary conditions

The simulation of the PCC desorption process was carried out on a 2-dimensional axisymmetric domain with boundary conditions (BC) as presented in Fig. 2. The aqueous loaded—with captured CO₂—MEA solution is supplied from a liquid source located above the porous regions of the column. Gases (CO₂ and water vapor) leave the stripper column at the top (gas outlet BC). The liquid collected in the bottom part of the stripper is heated by a heater (heat source BC). Porous zone BC reflects the real packing material (6 mm glass Raschig rings) applied in the reference laboratory installation.

During the model testing stage, the following simplifications were made:

- the height of the packing section was significantly reduced in order to decrease the computational time,
- heat transfer with surroundings was not considered.

The simulation was performed for the following values of key process parameters:

- liquid flux at stripper inlet: 50 l/h,
- liquid inlet temperature: 73°C,
- inlet solvent composition (mass concentrations): 80% water, 10% MEA-H, 10% MEA-CO₂,
- heater power: 2 kW.

The simulation was initialized with a gas phase composed of nitrogen only. The liquid phase collected at the stripper bottom was initialized with a 20% aqueous unloaded MEA solution at the temperature of 99°C (close to water boiling point). The above stated initial conditions reduced the computational time required to start the water evaporation process.

By default the process is highly unsteady with significant spatial local as well as temporal changes of the main physico-chemical process parameters. Hence it was decided to present the results for two different time moments: during start-up of the desorption process (for 0.5th s) and during the quasi-steady stage (for 10th s).

3. Results

Fig. 3 presents the gas temperature distribution in the form of a contour map. Liquid temperature distribution is not presented due to its similarity to the results of gas temperature.

As can be seen in Fig. 3, two regions can be identified in the stripper column:

- the region at the bottom of the column with uniform temperature of about 100°C,
- the region above the free liquid surface where a significantly smaller temperature occurs with a local minimum just below the porous zone.

The local temperature minimum is a result of endothermic character of desorption reaction. As a consequence of heat supply to the liquid bulk at the bottom of the column evaporation of the water takes place. It should be noted that since MEA and its relatives have a significantly higher boiling point

than water (boiling point at the atmospheric pressure for MEA is 172°C), it was assumed that they do not evaporate. In order to illustrate the unsteady character of the desorption process, temporal evolution of water evaporation in the form of mole fraction distribution of water vapor for first three seconds of the process is shown in Fig. 4. These results show how fast the evaporation process is, one may notice that local molar concentration of water vapour reaches even about 40%. It can also be observed that the processes occurring in the desorber column vary radically in character. In particular, significant molar concentration gradients can be observed close to the wall. This is a result of the heater being located in liquid bulk which is not attached to the column wall and there is a gap which is not directly affected by the heater. Therefore, water vapor does not evaporate from the entire liquid surface (see Fig. 4).

Contours of gas temperature under the quasi steady regime (10th second of the process) are shown in Fig. 5. The temperature distribution appears to have similar features as the results presented in Fig. 3 at the beginning of the process. The temperature inside the liquid bulk is locally slightly higher (about 4°C) and its local distribution is a result of changes in liquid density. It should also be noted that the local temperature minimum visible in Fig. 3 located just below the liquid source (for $t=0.5$ s) moves to the region between the liquid bulk and the porous region at the bottom of the column (for $t=10$ s). This can be explained as the liquid delivered to the column flows with reduced speed through the porous zone, and the axial position of the temperature minimum moves with the liquid front flowing down the column.

Special attention was paid to analysis of the temperature, due to its importance for the desorption process. The increase in temperature results from the rise in the reaction rate constant (see Eq. 7) which leads to the same increase in the overall reaction rate (see Eq. 6). Fig. 6 presents the axial distribution of the reaction rate of the desorption process. Dimensionless coordinate y in Fig. 6 represents the relative axial position in the column with $y=0$ and $y=1$ corresponding to the bottom and the top of the column, respectively. The most intense reaction occurs in the liquid bulk at the stripper bottom, where mo-

Table 1: Comparison of process efficiency indicators

working stage	efficiency $\eta_{des}, \%$	reboiler heat duty $E_{des}, \text{MJ/kg}$
start-up (1...3.5 s)	59	4.8
quasi-steady	100	2.9

lar concentrations of reactants reach the highest values (due to the absence of the gas phase). Moreover, reaction is accelerated in this region by temperature (see Fig. 5) according to Eq. 7. The reaction rate in the porous zone is much less intense (approx. 30 times lower than in the boiling liquid) mainly because of the low volume fraction of the liquid phase.

As a last element summarizing the simulation, an assessment of the efficiency of the desorption process is given through the use of two indicators:

- desorption efficiency,
- reboiler heat duty.

These two factors can be used to assess the quality and the cost-effectiveness of this CCS technology. The values of these two indicators were estimated for both the start-up period of system operation (in the range 1...3.5 s) as well as the quasi-steady state, and the results are summarized in Table 1.

The efficiency indicators of the process for the start-up period were determined on the basis of the values of CO_2 mass flow at the outlet of the column as well as the mass fraction of CO_2 in the exhaust gases; both these parameters were monitored during calculations. In the quasi-steady state, these values could be assumed to be constant in time.

Figure 7 presents the history of variation of mass flow of exhaust gases and CO_2 at the outlet of the column as well as the resultant mass fraction Y_{CO_2} . After about 3.5 s the mass fraction of CO_2 reaches about 0.8 and becomes stable. This is due to the almost complete removal of nitrogen from the column domain, which was initialized inside the column at the beginning of the calculations. As is visible from the analysis of contours collected in Fig. 4 presenting the evolution of the mole fraction of water vapor, after 3 s of the process, the front of the steam reaches

the outlet of the column and together with CO_2 almost entirely fills the column interior (see Fig. 7). It can be concluded that the values of both indicators: desorption efficiency and energy consumption must be far from optimal. However, after achieving a steady state they should reach significantly more favorable levels.

As can be seen from the data collected in Table 1, this trend in fact takes place, because the efficiency of capture rises significantly from 59% to 100% while the reboiler heat requirement decreases from 4.8 $\text{MJ/kg}_{\text{CO}_2}$ to 2.98 $\text{MJ/kg}_{\text{CO}_2}$. The values of these indicators achieved for a steady state differ significantly from typical levels for CO_2 capture systems.

Typical values of unit energy consumption given in the literature [21] are about 4.5 $\text{MJ/kg}_{\text{CO}_2}$, but in small-scale installations, the values of this parameter may be significantly higher. For example, in a laboratory CO_2 capture installation at the Institute for Chemical Processing of Coal (IChPW) in Zabrze [3], thermal energy consumption has to exceed even 10.5 $\text{MJ/kg}_{\text{CO}_2}$ to achieve CO_2 capture efficiency of 90%.

It can also be found in the literature that in laboratory and pilot CO_2 capture installations, the amount of MEA circulated in the circuit is several times greater than that implied by the stoichiometry of the desorption reaction [3]. This is dictated by economic analyses, which show that high efficiency CO_2 absorption is possible either by increasing column height (very expensive), or by using a suitably increased circulating stream of amine solution. The significantly increased flow rate of solvent needed to achieve desorption efficiency of above 90% is associated with a considerable increase in the power supplied to the desorber column [3].

As can be seen, the numerical model does not properly reflect the values of the efficiency of CO_2 desorption, and this can be caused by an incorrect assumption of the composition of the amine solution supplied at the desorber inlet (source). As shown by various pieces of research, the lean solvent at the stripper outlet contains unregenerated absorption products: MEA- CO_2 , MEA-H, while rich solvent (at the stripper inlet) includes a significant content of pure (CO_2 free) amine [22–25].

4. Conclusion

Based on the results of numerical simulations, the following conclusions can be drawn:

- the complex system of physico-chemical processes occurring in the stripper column was modeled relevantly, giving insight into the details of the desorption process,
- the functionality of the model, built as a set of user defined functions (UDFs), allows for its application to full scale installations,
- the unsteady simulation shows how desorption efficiency indicators are sensitive to key process parameters.

To sum up, the CFD model of the desorption process was elaborated, tested and together with a set of home made subroutines can be regarded as a useful numerical tool in parametric analysis of PCC technology.

The next step in developing and tuning the model will involve comparative studies using experimental data acquired at the laboratory CCS installation located at IChPW in Zabrze.

Acknowledgement

The results presented in this paper were obtained from research work co-financed by the National Centre of Research and Development in the framework of Contract SP/E/1/67484/10—Strategic Research Programme—Advanced technologies for energy generation: Development of a technology for highly efficient zero-emission coal-fired power units integrated with CO₂ capture.

Project DoktoRIS is kindly acknowledged for providing a scholarship to Mr. Niegodajew.

References

- [1] P. Niegodajew, D. Asendrych, Modelowanie przepływu przeciuprądowego gaz–ciecz w złożu porowatym, Vol. 14 of Modelowanie Inżynierskie, 2012.
- [2] D. Asendrych, P. Niegodajew, S. Drobniak, Cfd modelling of co₂ capture, Chemical and Process Engineering 34 (2013) 269–282.
- [3] A. Krótki, L. Więclaw-Solny, A. Tatarczuk, A. Wilk, D. Śpiewak, Badania laboratoryjne procesu absorpcji co₂ z zastosowaniem 30monoetanolaminy, Archiwum Spalania 12 (2012) 195–203.
- [4] P. Moser, S. Schmidt, S. Wallus, T. Ginsberg, G. Sieder, I. Clausen, J. Palacios, T. Stoffregen, D. Mihailowitsch, Enhancement and long-term testing of optimised post-combustion capture technology—results of the second phase of the testing programme at the niederaussem pilot plant, Energy Procedia 37 (2013) 2377–2388.
- [5] P. Moser, S. Schmidt, G. Sieder, H. Garcia, T. Stoffregen, Performance of mea in long-term test at the post-combustion capture pilot plant in niederaussem, Int. J. of Greenhouse Gas Control 5 (2011) 620–627.
- [6] T. Sonderby, K. Carlsen, P. Fosbol, L. K. G., N. von Solms, A new pilot absorber for co₂ capture from flue gases: Measuring and modelling capture with mea solution, International Journal of Greenhouse Gas Control 12 (2013) 18–192.
- [7] R. Dugas, P. Alix, E. Lemaire, P. Broutin, G. Rochelle, Absorber model for CO₂ capture by MEA application to CASTOR pilot results, Energy Procedia, 2008.
- [8] L. Remiorz, M. Brzęczek, Influence of ccs on efficiency of combined cycle power plants, Rynek Energii 106 (3) (2013) 81–86.
- [9] S. Jayarathna, B. Lie, C. Morten, M. Melaaen, Development of a dynamic model of a post combustion co₂ capture process, Energy Procedia 37 (2013) 1760–1769.
- [10] J. Milewski, J. Lewandowski, A. Miller, Reducing co₂ emissions from a gas turbine power plant by using a molten carbonate fuel cell, CHEMICAL AND PROCESS ENGINEERING-INZYNIERIA CHEMICZNA I PROCESOWA 29 (4) (2008) 939–954.
- [11] H. Ndiritu, K. Kibicho, B. Gathitu, Influence of flow parameters on capture of carbon dioxide gas by a wet scrubber, Journal of Power Technologies 93 (1) (2013) 9–15.
- [12] C. Alie, Co₂ capture with mea: Integrating the absorption process and steam cycle of an existing coal-fired power plant, Master’s thesis, University of Waterloo, Ontario, Canada (2004).
- [13] A. Kothandaraman, L. Nord, O. Bolland, H. Herzog, G. McRae, Comparison of solvents for post-combustion capture of co₂ by chemical absorption, Energy Procedia 1 (2009) 1373–1380.
- [14] A. Lawal, M. Wang, P. Stephenson, G. Koumpouras, H. Yeung, Dynamic modelling and analysis of post-combustion co₂ chemical absorption process for coal-fired power plants, Fuel 89 (2010) 2791–2801.
- [15] N. Harun, P. Douglas, L. Ricardez-Sandoval, E. Croiset, Dynamic simulation of mea absorption processes for co₂ capture from fossil fuel power plant, Energy Procedia 4 (2011) 1478–1485.
- [16] L. Simon, Y. Elias, G. Puxty, Y. Artanto, K. Hungerbuhler, Rate based modeling and validation of a co₂ pilot plant absorption column operating on mea, Chem. Eng. Research and Design 89 (9) (2011) 1684–1692.

- [17] L. Schiller, Z. Naumann, A drag coefficient correlation, Ver. Deutsch. Ing., 1935.
- [18] J. Maćkowiak, Fluid dynamics of packed columns, Springer Heidelberg Dordrecht London New York, 2010.
- [19] P. Vaidya, E. Kenig, Co₂-alkanolamine reaction kinetics: A review of recent studies, Chem. Eng. Technol. 30 (11) (2007) 1467–1474.
- [20] Z. Sun, M. Fan, M. Argyle, Desorption kinetics of the monoethanolamine/macroporous tio₂-based co₂ separation process, Energy & Fuels 25 (2011) 2988–2996.
- [21] Analiza możliwości poboru pary z układu siłowni do zasilania w ciepło instalacji separacji co₂, in: Mat. II Seminarium Projektu Strategicznego, Szczyrk, 2011.
- [22] R. Faiz, M. Al-Marzouqi, Mathematical modelling for the simultaneous absorption of co₂ and h₂s using mea in hollow fiber membrane contractors, Journal of Membrane Science 324 (2009) 269–278.
- [23] J. Gaspar, A.-M. Cormos, Dynamic modelling and validation of absorber and desorber columns for post-combustion co₂ capture, Comput. Chem. Eng. J. 35 (2010) 2044–2052.
- [24] P. Mores, N. Scenna, S. Musatti, Post-combustion co₂ capture process: Equilibrium stage mathematical model of the chemical absorption of co₂ into monoethanolamine (mea) aqueous solution, Chem. Eng. Res. Des. (2010) 1587–1599.
- [25] F. Ferrara, G. Cali, C. Frau, A. Pettinau, Experimental and numerical assessment of the co₂ absorption process in the sotacarbo pilot platform, in: 1st International Conference on Sustainable Fossil Fuels for Future Energy - S4FE, 2009.

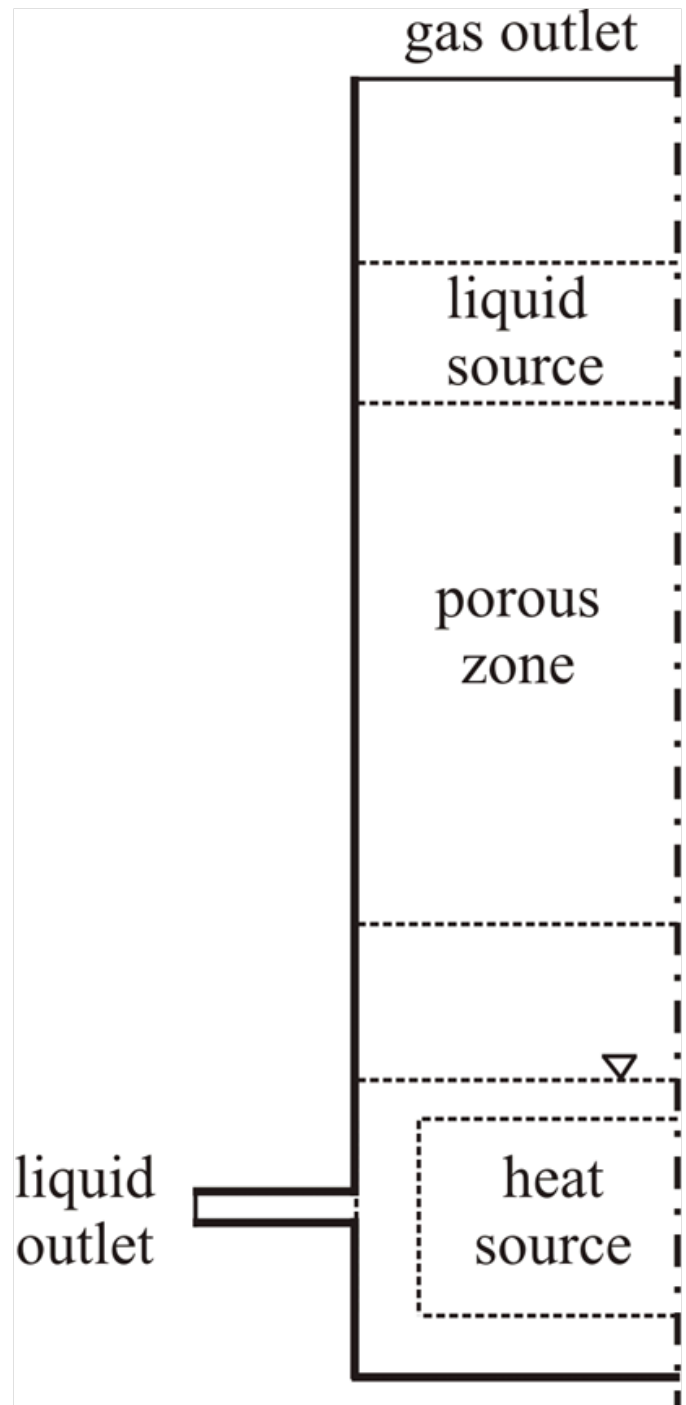


Figure 2: Schematic view of boundary conditions applied during simulation

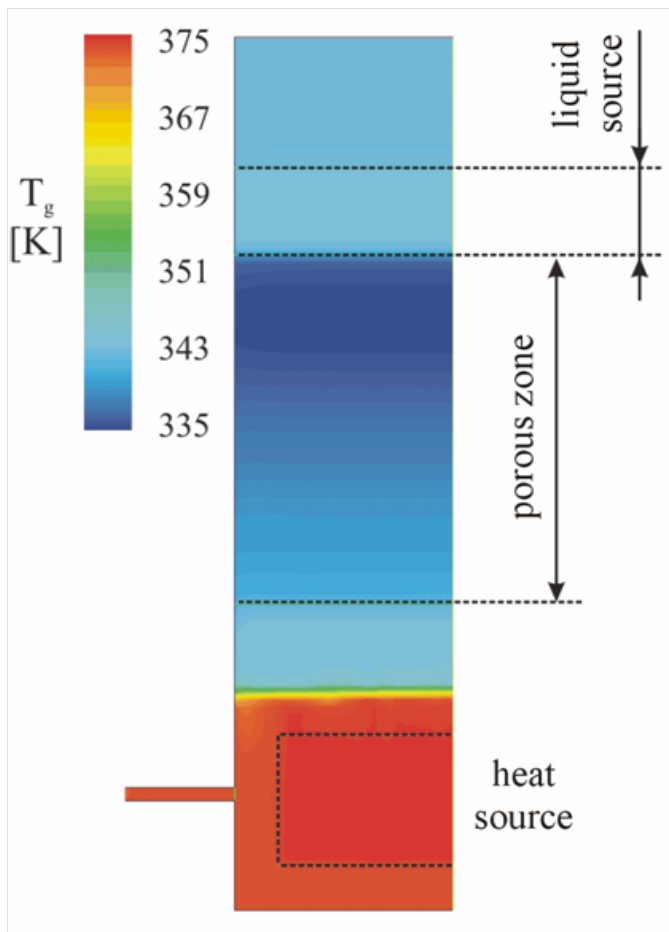


Figure 3: Contour map of gas temperature at 0.5 s after desorption initialization

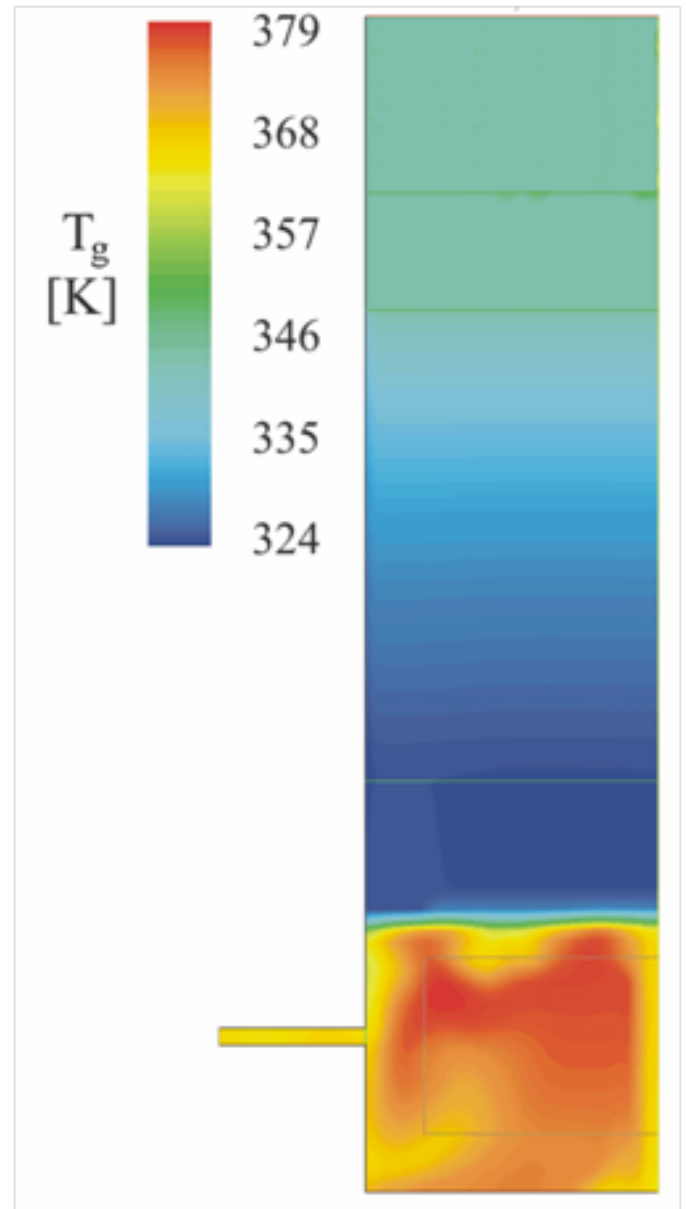


Figure 5: Contour of gas temperature for time 10s of the desorption process

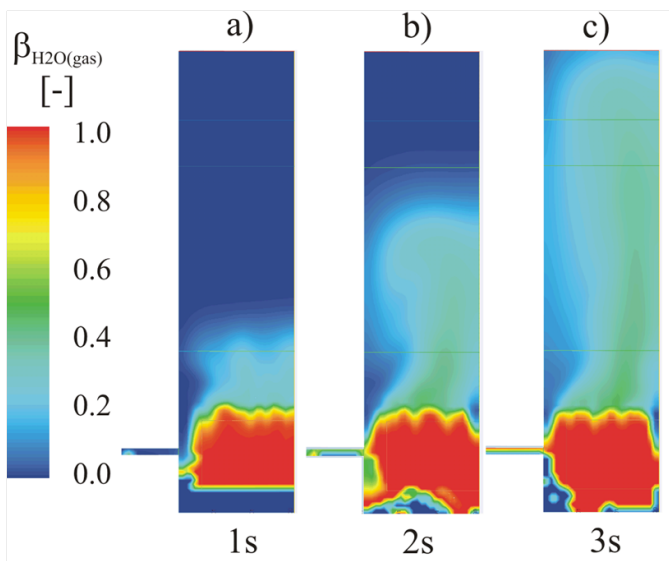


Figure 4: Contours of water vapor molar fraction in gas phase—evolution in time

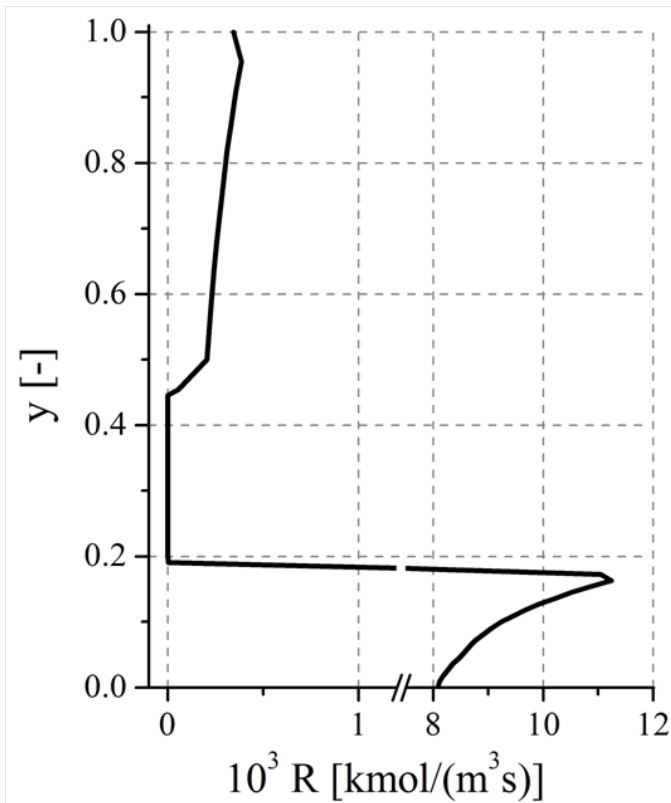


Figure 6: Axial distribution of reaction rate in desorber column

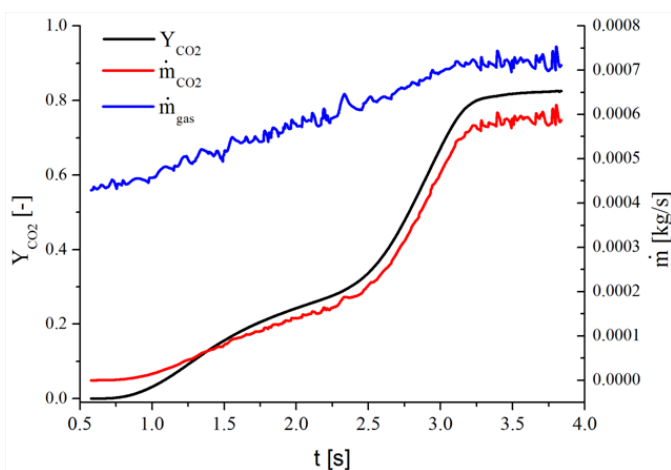


Figure 7: Time history of gas and CO₂ mass fluxes as well as CO₂ mass fraction in the exhaust gas (Y_{CO_2})